

## Antifungal activity of different size controlled stable silver nanoparticles biosynthesized by the endophytic fungus *Aspergillus terreus*

M.A. Mohamed<sup>1,2\*</sup>, H.M. Hussein<sup>3</sup>, A.A.M. Ali<sup>4</sup>

<sup>1</sup>Plant Pathology Research Institute, Agricultural Research Center, Giza 12655, Egypt

<sup>2</sup>Instituto de Biología Molecular y Celular de Plantas (Consejo Superior de Investigaciones Científicas - Universidad Politécnica de Valencia), Avenida de los Naranjos, 46022 Valencia, Spain

<sup>3</sup>Chemistry Department, Faculty of Science, Helwan University, Ain-Helwan, Cairo 11795, Egypt

<sup>4</sup>Plant Pathology Department, Faculty of Agriculture and Natural Resources, Aswan University, Aswan, Egypt

### Abstract

Silver nanoparticles (AgNPs) synthesized by using the aqueous extract of the endophytic fungus *Aspergillus terreus* F37 (KX024595) as reducing agent is reported here. The reaction medium employed in the synthesis process was optimized under a narrow range of pH and temperature to attain better yield, controlled size, and more stable of AgNPs. Further, the microbially synthesized AgNPs were studied through UV-vis spectroscopy, transmission electron microscopy (TEM), X-ray diffraction (XRD), and Fourier transform infrared (FT-IR) spectroscopy analyses. The obtained results indicated the formation of high crystalline spherical AgNPs with an average diameter of  $45.2 \pm 0.5$  nm at room temperature (22 °C). Quantitative analyses indicated that reduction of the Ag<sup>+</sup> precursor was promoted at elevated pH due to increased activity of biomolecules in the fungal extract. As a result, the size of the AgNPs decreased with increased pH of the reactions. The optimum conditions for maximum production of small control sized AgNPs ( $12 \pm 0.5$  nm) were pH (10) and temperature (100 °C). The outcomes of the antifungal activity of different controlled sized AgNPs showed their efficiently to inhibit the mycelial growth of the pathogenic fungus *Alternaria solani*, the causal agent of tomato early blight disease and reduced their viability in a pH and temperature dependent manner. These findings revealed that the fine tuning of the reaction synthesis parameters, will increase the chance to obtain desired well shaped and small sized AgNPs with potent antifungal activities, may have important applications as new bio-fungicides in controlling various plant diseases caused by fungi.

**Keywords:** silver nanoparticles, size control, pH, biosynthesis, *Aspergillus terreus*, antifungal activity.

\* Corresponding author: M.A. Mohamed,  
Tel: +201018274608, Fax: +20882342708,  
E-mail: [mohammed\\_sharouny@yahoo.com](mailto:mohammed_sharouny@yahoo.com)

## Introduction

Silver nanoparticles (AgNPs) have been widely studied during the past few decades due to their unique optical and electric properties and potential applications in electronics (Evanoffand & Chumanov, 2004), catalysis (Mohamed et al. 2016; Mallick & Witcomb, 2006), bio-labeling (Zhang et al., 2005; McFarland & Van Duyne, 2003), and also and also biotechnology (Khatami et al., 2018; Abd-Alla et al., 2016; Kathiravan et al., 2015; Iravani, 2011). The AgNPs are also well known to exhibit a broad spectrum of biocidal activity towards many bacteria, fungi and viruses (Cordero et al., 2017; ; Abd-Alla et al., 2016; Kumar & Sujitha, 2014; Zachariadis et al., 2004). Interestingly, the antimicrobial effect of AgNPs is size dependent, where as their size is smaller as the antimicrobial effect is more potent (Morones et al., 2005). Hence, extensive works have been carried out to synthesize silver nanoparticles with controllable shape and size desired (Lu et al., 2006; Wiley et al., 2006; Ni et al., 2005; Sherry et al., 2005). Reduction of the silver salt precursor ( $\text{AgNO}_3$ ) by chemical reductants such as citrate (Pillai & Kamat, 2004), ascorbic acid (Sondi et al., 2003; Velikov et al., 2003), or sodium borohydride (Ahmadi et al., 1996) is among the most used methods for the synthesis of AgNPs in aqueous solution. However, the AgNPs produced by the citrate reduction route were usually tend to exist in mixtures of different shaped (e.x spherical and rod-like) due to the poor balance of nucleation and growth processes (Dong et al., 2009) and those produced by sodium borohydride were usually small spherical silver nanoparticles (<10 nm) due to the high reactivity of the borohydride (the reductant) which may lead to induce the explosive nucleation process. So, it is less

productive to tune the nucleation and growth processes and thus the size of the AgNPs by changing the reaction parameters such as molar ratio of the reductant/silver precursor, pH, or temperature of the reactions when citrate or sodium borohydride was employed as the reductants in the synthesis process. Also, involving such reductans like borohydride in the AgNPs synthesis cause environmental toxicity or biological hazards which limits its applications in human being applications. By taking all together in parallel with LaMer model (Ji et al., 2007), a reasonable way to prepare silver nanoparticles with tunable size is to choose a reductant with suitable reactivity and safe impact to mediate the nucleation and growth processes of the particles. In another hand, Qin et al. (2010) reported a dependence between size and pH of the reaction system, as pH of the reaction mixture is increased, the average size of the AgNPs was decreased (Reddy et al., 2014). This stimulates the scientists to search out clean, non-toxic and environmentally acceptable biological routes for the synthesis of AgNPs (Escárcega-González et al., 2018; Mittal et al., 2013; Qian et al., 2013). Fungi are a good option compared to other eukaryotes because of the vast repertoire of proteins, enzymes, and other bioactive secondary metabolites that they produce, which possess redox capacity and, thus, increase productivity during the biosynthesis process (Abdel-Hafez et al. 2016 a,b; Mohamed 2015; Phithiviraj et al. 1998). These biomolecules serve as reducing agents to reduce various silver salts to its corresponding zero valent metallic nanoparticles and also as stabilizing agents to prevent nanoparticles from agglomeration. Moreover, the biosynthesis route has not only resulted in environmental benefits, but also enhances their physico-chemical

property, which leads to more effective application (Morsy et al., 2014; Liu et al., 2013; Tanvir et al., 2012). Although silver nanoparticles are effective against a number of phytopathogenic fungi including *Bipolaris sorokiniana* and *Magnapothe grisea* (Shrivastava et al., 2007; Panacek, et al., 2006; Morones et al., 2005), however many phytopathogenic fungi are not explored although they are causing destructive diseases on important crop plants and thereby reducing the yield of agricultural products. *Alternaria solani* (Ellis & Martin) Jones & Grout is a soil inhabiting, air-borne fungal pathogen responsible of tomato early blight disease, one of the most important and frequent fungal disease infecting tomato crops worldwide, causing reduction in tomato crop quantity and quality (Song et al., 2011). Our aim in the present work was to biosynthesize AgNPs using the endophytic fungus *Aspergillus terreus* F37 (KX024595), to characterize them under a range of pH and temperature values and to test their antifungal activity against three different pathogenic isolates of *Alternaria solani* the causal agent of tomato early blight disease.

## Materials and methods

**Sample collection and isolation of endophytic fungi:** Four hundreds of fresh healthy tomato (*Solanum lycopersicum* L.) leaf plants were collected from Egypt in 2015 to isolate endophytic fungi. The collected samples were transferred directly to the mycological laboratory, Botany and Microbiology Department, Assiut University, Egypt. At laboratory, leaves were gently washed with running tap water and aseptically cut into small segments (5 × 5 mm). All segments were

rinsed with distilled water and surface sterilized following the sequence: 70% ethyl alcohol for one minute, and then transferred to a solution of 2.5% sodium hypochlorite for 3.5 min, followed by a treatment with 70% ethanol for 30 s. the prepared segments were then put on Petri dishes containing potato dextrose agar (PDA) medium containing 250 mg L<sup>-1</sup> streptomycin and incubated at 26 ± 2 °C for 8 days. The hyphal tips of the fungal endophytes growing out from the plant tissues were carefully transferred onto new PDA plates under sterilized conditions and incubated at 26 ± 2 °C for 8 days. After incubation, fungal endophytes identification was performed according to morphological characteristics. Percent colonization frequency (% CF) of endophytic fungi was calculated according to Petrini and Fisher (1988): colonization frequency (%) = (total number of segments colonized/ total number of segments) × 100.

**DNA extraction:** The frozen mycelia of the fungus (100 mg) were ground with liquid nitrogen in a mortar and pestle and mixed with 1 ml of 4 M guanidinium thiocyanate, 0.1 M sodium acetate pH 5.5, 10 mM ethylenediaminetetraacetic acid (EDTA), 0.1 M 2-mercaptoethanol. Extracts were clarified by centrifugation and supernatants were loaded into silica gel spin columns (Wizard Plus SV Minipreps DNA Purification, Promega, USA). Columns were washed with 70% ethanol, 10 mM sodium acetate pH 5.5, and DNA eluted with 50 µl of 20 mM Tris-HCl, pH 8.5.

**Ribosomal DNA amplification and sequencing:** A ribosomal internal

transcribed spacer (ITS) was amplified by PCR using primer pairs ITS1 (5'-CTTGGTCATTTAGAGGAAGTAA-3') and ITS4 (5'-TCCTCCGCTTATTGATATGC-3') (Gardes & Bruns, 2012). Fungal DNA (1  $\mu$ l) was amplified in a 20- $\mu$ l reaction with 0.4 U Phusion DNA polymerase (Thermo Scientific) in the presence of 0.2 mM dNTPs, 3% dimethyl sulfoxide, 0.5  $\mu$ M of each primer and HF buffer (Thermo Scientific). The reaction consisted in an initial denaturation for 30 s at 98°C, followed by 30 cycles of 10 s at 98°C, 30 s at 55°C and 30 s at 72°C, and a final extension of 10 min at 72°C. PCR products were separated by electrophoresis in a 1% agarose gel run for 75 min in TAE buffer (40 mM Tris, 20 mM sodium acetate, 1 mM EDTA, pH 7.2) and viewed using a UV transilluminator after ethidium bromide staining. According to electrophoretic migration, the PCR products that corresponded to the ribosomal ITS were eluted from the gel using silica spin columns (DNA Clean & Concentrator, Zymo Research). Both strands of the amplified ribosomal ITS DNA were sequenced using primers ITS1 and ITS4. The consensus sequences were employed to search for homologous sequences with the BLAST search program at the National Center for Biotechnology Information (NCBI: <http://www.ncbi.nlm.nih.gov>).

**Extracellular synthesis of AgNPs:** For the biosynthesis of AgNPs using an extract of the endophytic fungus *A. terreus*, Ten mg (dry weight) of the fungal mycelia was brought in contact with 100 mL of sterilized double distilled water in a 250 mL Erlenmeyer flask and

agitated at 120 rpm for 48 h at 26 °C  $\pm$  2. After the incubation, the cell filtrate was obtained by filtering it through Whatman filter paper No. 1. The filtrates were treated with 1 mM silver nitrate (AgNO<sub>3</sub>) solution in an Erlenmeyer flask and incubated at room temperature (~22 °C) in dark. Cell-free filtrate without silver nitrate solution was also run as control.

**Characterization of AgNPs:** The mycosynthesized AgNPs were characterized by UV-vis spectroscopy periodically for 1 month in order to observe the formation of stable AgNPs by the action of the fungal extract. Small aliquots (2 mL) of the colored suspended AgNPs were loaded in a quartz cuvette and analyzed using A PerkinElmer Lambda 950 UV/Vis spectrometer through a wavelength scanning ranging between 300 and 800 nm at different time intervals with distilled water as a reference. The AgNPs solution was then centrifuged at 14000 rpm for 15-20 min. The supernatant was discarded and the pellets were dispersed with distilled water, washed 3 times with de-ionized distilled water to remove the free entities and unbound biological molecules from AgNPs, and was finally dried at 60 °C .

**High-resolution transmission electron microscopy (HR-TEM):** For the HR-TEM measurements, a drop of thin dispersion (~3  $\mu$ L) AgNPs sample dispersed in double distilled water was drop coated on carbon grid (carbon type-B, 300 mesh, Ted Pella, Inc., Redding, CA, USA). After about 20 min, the grid was removed and air dried and the images of nanoparticles were studied using High Resolution-Transmission Electron Microscopy (HR-TEM) assisted

with Energy dispersive X-ray spectroscopy (EDS). The hydrodynamic diameter and the zeta potential of the AgNPs were also measured by dynamic light scattering (DLS) using a Malvern Zetasizer Nano ZS 90 (Worcestershire, UK).

**X-ray diffraction (XRD) pattern and energy-dispersive X-ray spectroscopy (EDS) analyses:** Crystalline metallic pattern of AgNPs powder was analyzed using X-ray diffraction patterns. The X-ray diffraction (XRD) patterns were conducted on Bruker AXS D8. Advance X-ray diffractometer operated at a voltage of 40 kV and a current of 40 mA with Cu K( $\alpha$ ) radiation and wavelength 1.541 $\text{\AA}$ . The scanning was done in the region of  $2\theta$  from 20 to 80. The EDS analysis was performed to identify the elemental composition of the biosynthesized AgNPs using INCA Energy TEM 200 with the JEOL analysis software.

**Fourier transform infrared spectroscopy (FTIR):** The FTIR analysis of the dried AgNPs powder mixed with a pinch of potassium bromide (Himedia FTIR graded) in a crucible was made into pellet by hydraulic press and the pellet spectrum was then recorded using a JASCO FT/IR-6300 Fourier transform infrared spectrometer equipped with a JASCO IRT-7000 Intron Infrared Microscope, using transmittance mode operating at a resolution of 4  $\text{cm}^{-1}$  (JASCO, Tokyo, Japan) (Siddique et al., 2013).

**Optimization of silver nanoparticles size:** In an attempt to produce better size controlled AgNPs, the effect of

parameters such as, pH and temperature with different incubation time was studied by varying one parameter at a time, keeping the other experimental conditions the same. In all the reactions, the concentrations of silver nitrate and the fungal extract acid were set as 1 mM and 10 g (wet weight) of fungal mat / 100 mL respectively. The mixtures were incubated at different pH values (5-11) and temperatures (25-100  $^{\circ}\text{C}$ ) for various time periods for one month with respect to AgNPs stability. By simply varying the pH and temperature of the reaction system, we can tune the size of the nanoparticles. When the reaction is completed, products were collected and thoroughly washed for several times with ethanol to obtain pure AgNPs without any by-products and finally subjected to vacuum dry at 80  $^{\circ}\text{C}$  for 3 h. The optimum of reaction parameters were then selected by measuring the absorbance of the resulting solutions spectrophotometrically using a UV-visible spectrophotometer (Lambda 35 $\text{\textcircled{R}}$ -PerkinElmer, Waltham, MS, USA) operated at a resolution of 1 nm and scanned in the wavelength range of 300–800 nm. For each condition, respective controls were maintained. The hydrodynamic diameter of the AgNPs were measured by dynamic light scattering (DLS) using a Malvern Zetasizer Nano ZS 90 (Worcestershire, UK).

**Antifungal assay of controlled sized AgNPs:** The antifungal activity of AgNPs was measured on three pathogenic isolates of *Alternaria solani* by the agar dilution method. Plates were supplemented with three concentrations (5, 10, and 20 ppm) from each biogenic

AgNPs (biosynthesized under room and optimum conditions). A disc (1.5 cm) of mycelial growth of the phytopathogenic fungus *Alternaria solani*, taken from the edge of 8 day old fungal culture, was placed in the center of each plate. The inoculated plates were then incubated at  $25\text{ }^{\circ}\text{C} \pm 1$  for 8 days. The antifungal activity was then evaluated by measuring the radial growth of fungal colonies (Kim et al. 2012; Kim et al, 2009):

$$\text{Inhibition rate (\%)} = \frac{R - r}{R} \times 100$$

Where,  $R$  is the radial growth of the fungal hyphae on the control plate and  $r$  is the radial growth of the fungal hyphae on the plate supplemented with AgNPs. All experiments were conducted in triplicate under sterile conditions.

## Results and Discussion

**Identification of endophytic fungi in tomato leaves:** From the 400 analyzed healthy tomato leaves, 19 fungal species in addition to 4 morpho taxa belonging to 11 genera were isolated (Table 1). Fungal species were identified according to their morphological characters. The most predominant species was *Cladosporium sphaerospermum*, *Trichoderma harzianum*, *Aspergillus terreus* which showed 30.25%, 27.5%, 25.5% colonization frequency respectively. *Aspergillus terreus* (Figure 1) is considered one of the most important fungal species that produce bioactive secondary metabolites (Dewi et al., 2014), which is why we decided to focus our next work on this fungus isolate. The

molecular identification of both the endophytic *A. terreus* and three pathogenic isolates of *Alternaria solani* was confirmed by sequence analysis of the nuclear ribosomal ITS region. The sequence of a 623 base pair DNA fragment corresponding to the ITS1-5.8S-ITS2 region supported the identification of the endophytic fungus as *A. terreus* F37 (KX024595), showing 100% identity with the sequence of the *Aspergillus terreus* strain MF12 (JF431429). The same for the three pathogenic *Alternaria solani* isolates. A partial 18S rRNA gene sequence of approximately 624 base pairs of *Alternaria solani* F11 (KT721909), *Alternaria solani* F12 (KT721910) and *Alternaria solani* F14 (KT721911) had a sequence with 100% identity to that of pathogenic *Alternaria solani* KT6 (F02664) available in the GenBank database.



Figure 1: The isolated endophytic fungus *Aspergillus terreus*: Microscopic features showing the fungal morphology.

Table 1: The composition of the isolated endophytic fungal taxa and frequency of colonization (%) per 400 segments of healthy tomato leaves.

| Fungal endophytes                                      | No. of records | Frequency (%) |
|--|----------------|---------------|
| <i>Alternaria alternata</i> (Fr.) Keissler             | 35             | 8.75          |
| <i>Alternaria solani</i> Sorauer                       | 1              | 0.25          |
| <i>Aspergillus niger</i> van Tieghem                   | 2              | 0.5           |
| <i>Aspergillus tamari</i> Kita                         | 3              | 0.75          |
| <i>Aspergillus terreus</i> Thom                        | 102            | 25.5          |
| <i>Aspergillus versicolor</i> (Vuill.) Tiraboschi      | 20             | 5             |
| <i>Chaetomium globosum</i> Kunze                       | 67             | 16.5          |
| <i>Cladosporium cladosporioides</i> (Fr.) De Vries     | 80             | 20            |
| <i>Cladosporium oxysporum</i> Link                     | 35             | 8.75          |
| <i>Cladosporium sphaerospermum</i> Penzig              | 121            | 30.25         |
| <i>Curvularia lunata</i> (Wakker) Boedijn              | 5              | 1.25          |
| <i>Emericella</i> sp.                                  | 4              | 1             |
| <i>Epicoccum nigrum</i> Link ex Schlecht               | 100            | 25            |
| <i>Fusarium oxysporum</i> Schlecht                     | 77             | 19.25         |
| <i>Fusarium solani</i> (Mart.) Sacc.                   | 11             | 2.75          |
| <i>Myrothecium verrucaria</i> (Albert. & Schw.) Ditmar | 3              | 0.75          |
| <i>Penicillium chrysogenum</i> Thom                    | 55             | 13.75         |
| <i>Penicillium commune</i> Thom                        | 4              | 1             |
| <i>Trichoderma harzianum</i> Rifai                     | 110            | 27.5          |
| Morphotaxon 1  | 2              | 0.5           |
| Morphotaxon 2  | 2              | 0.5           |
| Morphotaxon 3  | 5              | 1.25          |
| Morphotaxon 4  | 2              | 0.5           |

### Biosynthesis of AgNPs using the endophytic fungus *Aspergillus terreus*:

Next, we went on to analyze the possibility of biosynthesizing AgNPs using the fungal extract of *A. terreus* F37 (KX024595). The possibility of AgNPs biosynthesis using a fungal extract of the endophytic fungus *Aspergillus terreus* F37 (KX024595) was confirmed by observing the color change of AgNO<sub>3</sub> solution after challenging with the fungal extract. The UV-vis absorption spectrum showed a strong absorption peak centred at 430 nm at different time intervals, which is characteristic of surface

plasmon resonance of silver (Abdel-Hafez et al., 2016a; Mohamed, 2015; Azizi et al., 2013; Borneman & Hartin, 2000), and hence indicated the formation of AgNPs (Figure 2A). Moreover, the continued increase in the AgNPs absorbance was observed with a prolonged reaction time, which indicated a continued reduction of silver ions and the production of more stable AgNPs.

**Characterization of AgNPs:** The size and morphology of the biosynthesized AgNPs were examined using HR-TEM. The measurements indicated the

formation of spherical shaped AgNPs with average size distribution of  $45.2 \pm 0.5$  nm (Figure 2B, C). Moreover, the negative zeta potential of the AgNPs was about  $-35.2 \pm 1.0$  mV that suggests an

ideal surface charge of the formed AgNPs, Which prevent the particles agglomeration and generate a strong repulsive force among the particles that increase their stability (Figure 3).

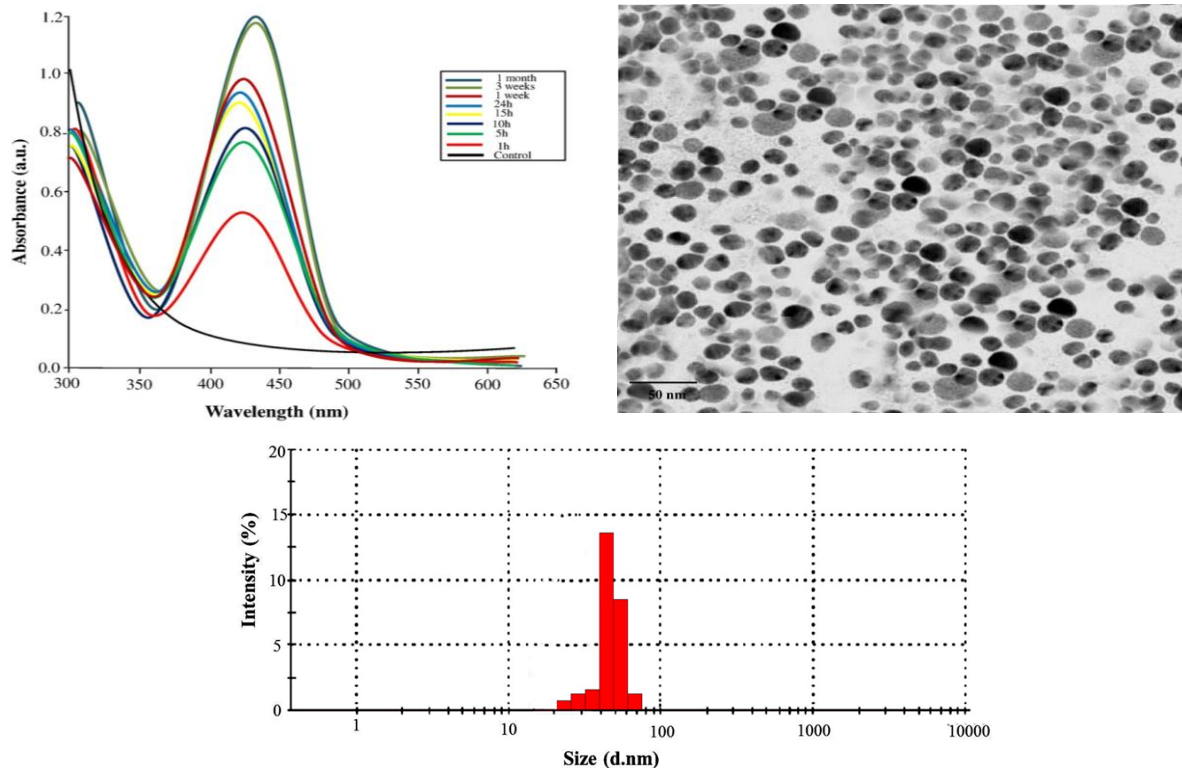


Figure 2: Characterization of the silver nanoparticles synthesized by the reduction of  $Ag^+$  using *A. terreus* fungal extract: (A) UV-vis spectra of the AgNPs at different time intervals, (B) HR-TEM image of the AgNPs synthesized showing a general view of well-dispersed spherical AgNPs. (C) DLS measurement of the formed AgNPs.

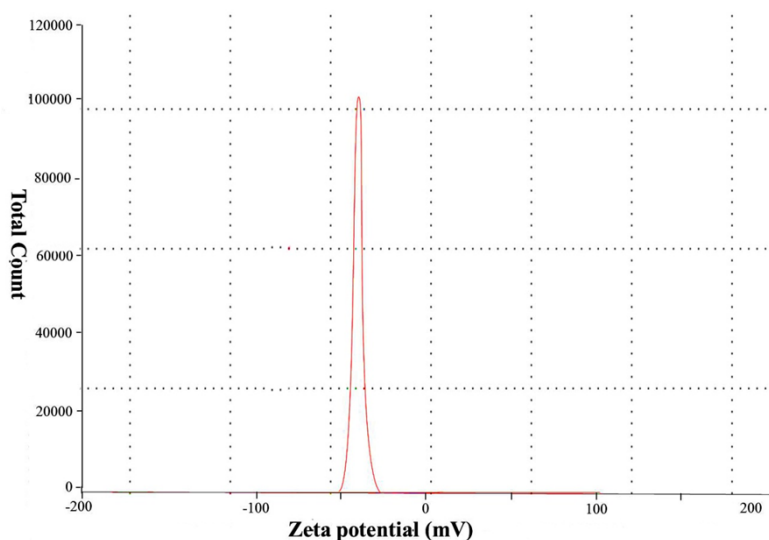


Figure 3: Zeta potential analysis of the formed AgNPs.

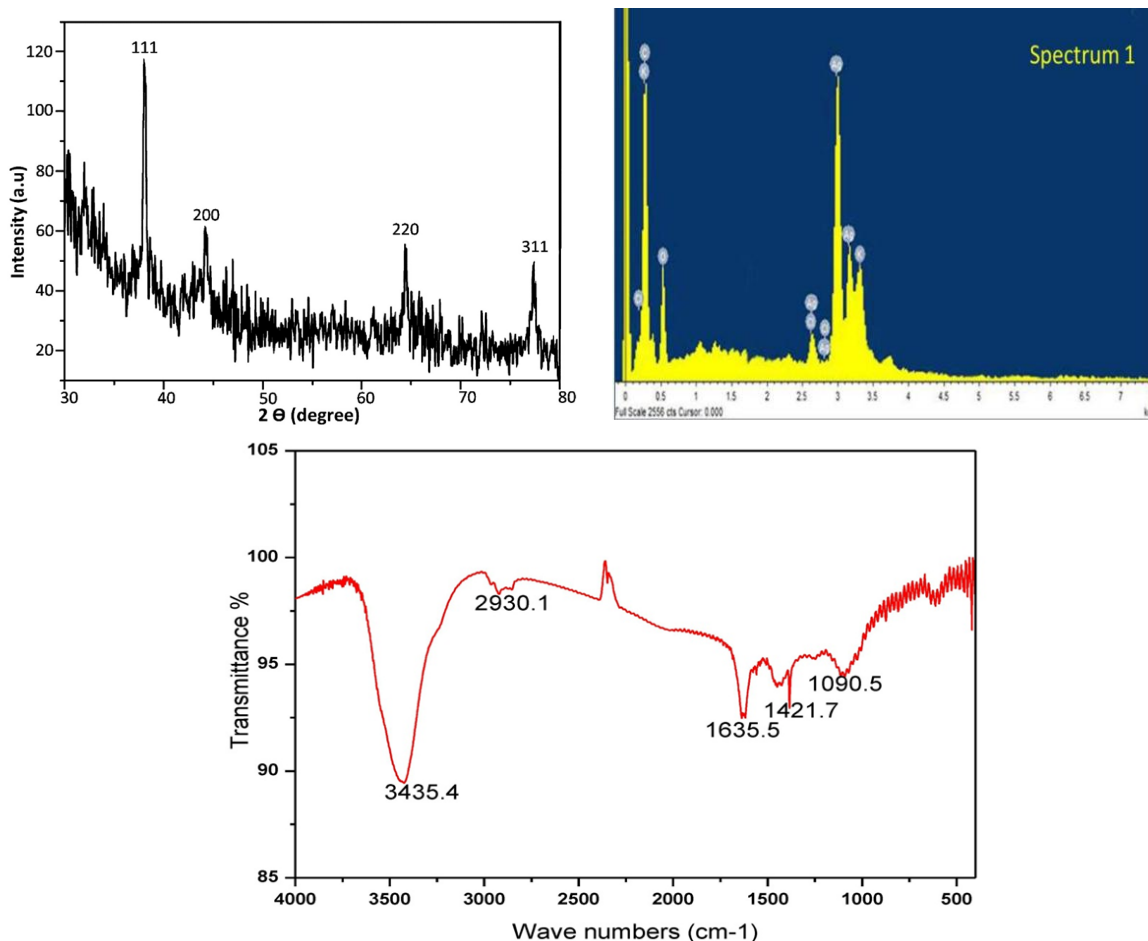


Figure 4: Characterization of AgNPs by spectroscopic analyses: (A) X-ray diffraction patterns of synthesised Ag NPs, (B) EDS spectroscopy displaying the purity and chemical composition of the biosynthesised AgNPs. (C) The FTIR spectra of the synthesised AgNPs.

The XRD pattern revealed the typical fcc structure of AgNPs. The XRD spectra showed four main characteristic Bragg diffraction peaks at  $2\theta$  values of nearly  $37^\circ$ ,  $44.2^\circ$ ,  $64.3^\circ$ , and  $77.8^\circ$  which correspond to (111), (200), (220), and (311) planes respectively of fcc silver nanoparticles (Figure 4A). The diffraction peaks were consistent with standard database files (JCPDS card No 04-0783), indicating that the synthesized nanoparticles were of pure crystalline in nature. The EDS spectrum showed a strong typical optical absorption peak at approximately 3 keV, which was

attributed to the Surface Plasmon Resonance (SPR) of the metallic Ag nanocrystals and confirm the significant presence of pure metallic Ag (Figure 4B) (Azizi et al., 2013). The FT-IR spectrum was carried out to identify the possible functional groups present in the fungal extract, which may play as capping and reducing agents in the formation of AgNPs. As shown in (Figure 4C), the IR spectrum displays intense bands at  $3435.4\text{ cm}^{-1}$ ,  $2930.1\text{ cm}^{-1}$ ,  $1635.5\text{ cm}^{-1}$ ,  $1421.7\text{ cm}^{-1}$  and  $1090.5\text{ cm}^{-1}$ . The broad band at  $3435.4\text{ cm}^{-1}$  corresponds to the strong stretching vibrations of hydroxyl

(-OH) group of phenolic compounds present in the fungal extract. The intense peak at  $2930.1\text{ cm}^{-1}$  corresponds to C-H stretch band of alkanes. The intense peaks at  $1701\text{ cm}^{-1}$  can be attributed to the  $\text{-C=O-}$  and  $\text{-C=C-}$  stretching vibrations, which indicates the presence of flavonoids and terpenoids and proteins in the fungal extract of *A. terreus*. The medium absorption peak located at  $1635.5\text{ cm}^{-1}$  can be identified as the amide group. This amide band occurs due to carbonyl stretch and N-H deformation vibrations in the amide linkage of proteins. It is well known that the metallic ions can bind to carboxylic groups and therefore this reveals opens the possibility of AgNPs bound to proteins through the carboxyl groups. The band at  $1421.7\text{ cm}^{-1}$  and  $1090.5\text{ cm}^{-1}$  corresponds to the C=N stretching vibration and C-N stretch of aromatic and aliphatic amines respectively. Thus, taking all together, these observations support that the formed AgNPs are

suggested to be surrounded with proteins and secondary metabolites containing amine, alcohol, ketone and carboxylic acid functional groups which may be responsible to their stability.

#### Optimization of the AgNPs synthesis conditions:

The color of reaction mixture and the intensity of the absorbance peaks were pH dependent. The AgNPs synthesized at pH of 5.0, 6.0, 7.0, 8.0, 9.0, 10.0 and 11.0 presented absorption peaks at 520, 470, 440, 435, 430, 425, and 420 nm respectively (Figure 5). The absorption peaks shifted to shorter wavelength and became narrower at higher pH values, possibly due to the decreased size or anisotropy degree of AgNPs (Noguez, 2007; Slistan-Grijalva et al. 2005; Evanoff & Chumanov, 2004). TEM and DLS measurements were carried out to observe the size and morphology of the AgNPs prepared under different pH values (Figures 6 and 7)

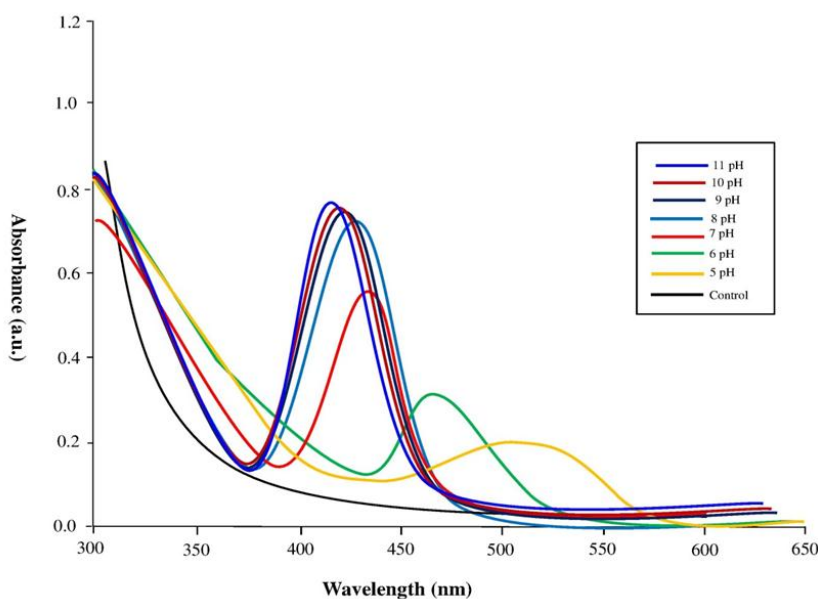


Figure 5: Optimization of AgNPs under different pH values.

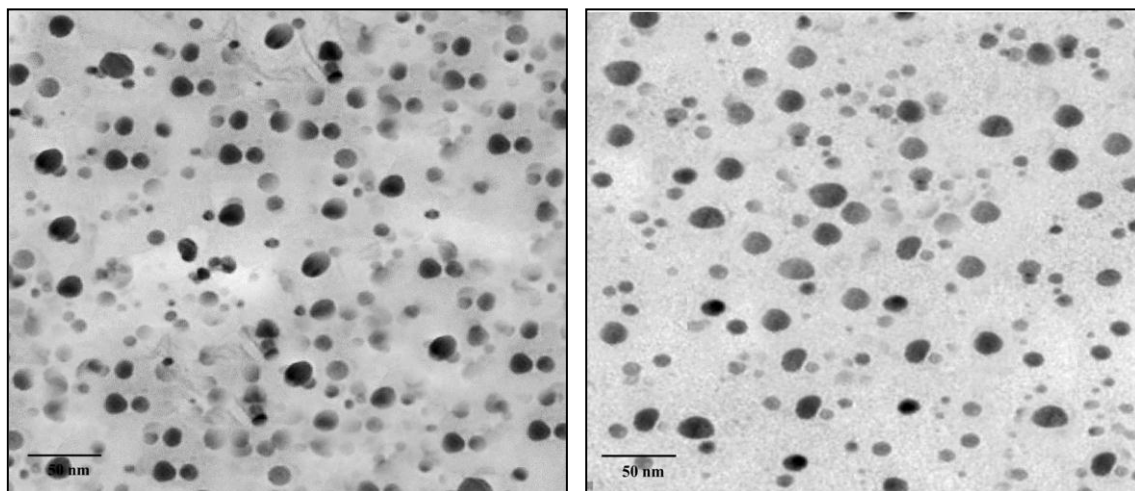


Figure 6: Characterization of AgNPs under different pH values: HR-TEM images of AgNPs at (A) pH= 9, (B) pH=10.

As shown in Figure 6 (A, B), all the particles prepared were spherical in shape. The shape of the formed AgNPs prepared under lower pH (5.0-6.0) was less regular. The smallest particle size was produced at pH 9 and 10 with  $37 \pm 0.5$  nm and  $30.5 \pm 1.5$  nm respectively (Figure 7 A, B). Particles obtained at pH 7 were significantly of larger size,  $45.2 \pm 0.5$  (Figure 2B). In acidic

conditions we cannot observe any characteristic absorbance band for AgNPs formation. These results revealed that the optimum pH value for maximum production of small size AgNPs is 10. At pH 11, we did not observe further increase in absorbance intensity or decrease in AgNPs. These results are in agreement with previous findings (Baghizadeh et al., 2015).

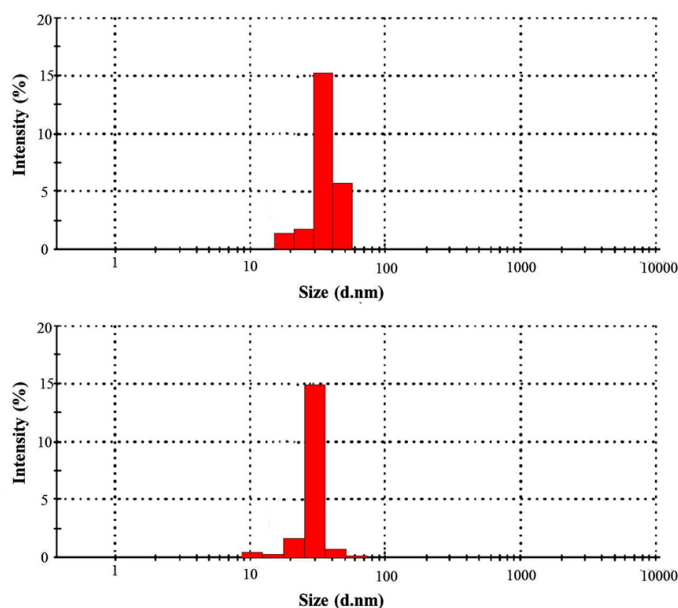


Figure 7: Characterization of AgNPs under different pH values: DLS measurements of AgNPs at (A) pH= 9, (B) pH=10.

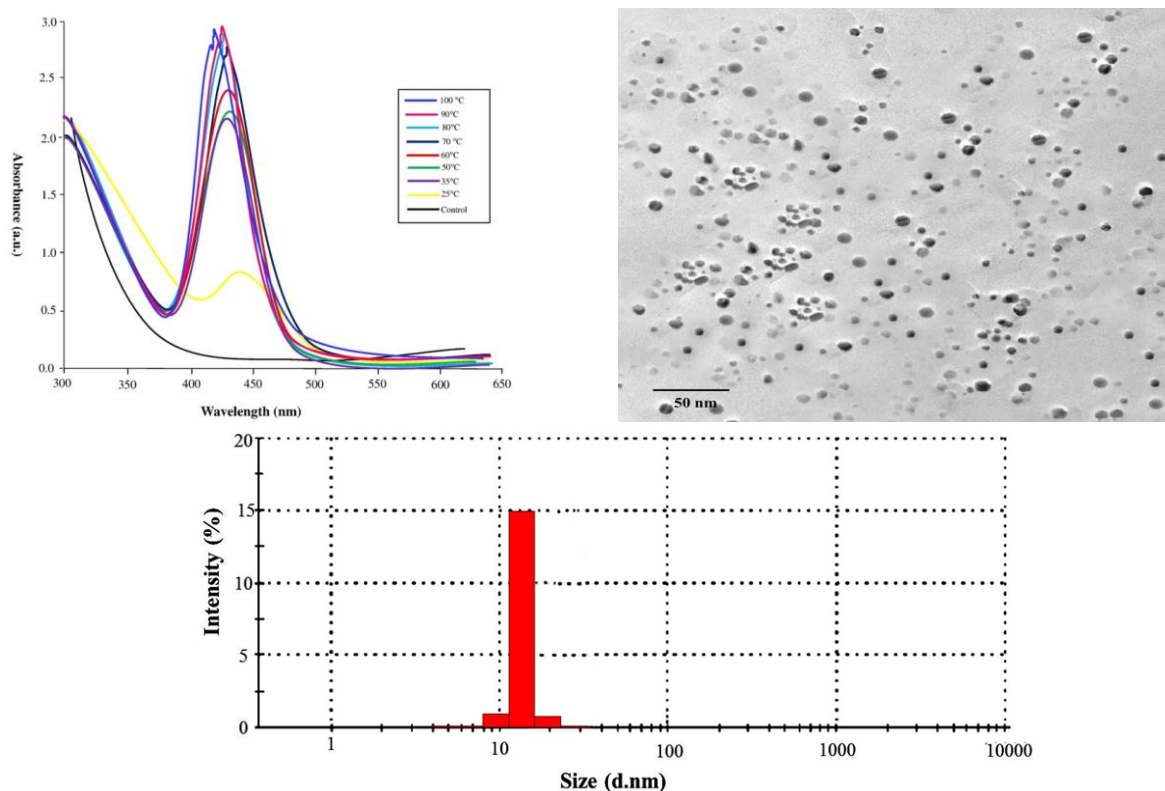


Figure 8: Optimization of AgNPs under different Temperature values: (A) Uv-absorbance of the formed AgNPs under different Temperature values, (B) HR-TEM image of AgNPs under 100 °C temperature, (C) DLS measurement of the optimized AgNPs under 100 °C.

Other studies reported that at pH 2.0, no reaction occurred while at pH 7-11, highly and small sized mono-dispersed nanoparticles were obtained (Roopan et al., 2013). While the effect of pH on the production of controlled small sized AgNPs was being investigated, the smallest AgNPs ( $30.5 \pm 1.5$  nm) obtained at pH 10 were also subjected to a range of temperatures degrees (20, 40, 60, 70, 80, 90 and  $100^{\circ}\text{C}$ ) to study the effect of the reaction temperature on AgNPs size. The UV results indicated a noticeable absorbance increase with increasing the temperature degree (Figure 8A). Moreover, UV spectra showed sharp narrow peaks at slightly lower wavelengths (430 and 425 nm) at

increasing temperatures (90 and  $100^{\circ}\text{C}$ , respectively). This means that there is a linear relationship between the maximum absorbance and the temperature which actually accelerate the AgNPs production to the optimum state. As shown in Figure 8B, all the particles prepared were spherical in shape. The smallest particle size of AgNPs are exactly produced ( $12 \pm 0.5$  nm) after transferred into a  $100^{\circ}\text{C}$  water bath for 1 h (Figure 8C). These results suggest that when the temperature is increased, the reactants are consumed more rapidly leading to the formation of smaller nanoparticles (Baghizadeh et al., 2015). In order to evaluate the stability of the AgNPs in an aqueous system, the

absorption spectrum was recorded after storage at room temperature for 3 months. As shown in Figure 9, the absorption peak of the formed AgNPs shifted slightly from 430 to 440 nm, but no significant changes in peak intensity were observed. This suggests acceptable stability of AgNPs for at least 30 days at room temperature.

**Antifungal activity of sized controlled AgNPs:** After formation AgNPs under room and optimum conditions and generate nanoparticles with different controlled size, we studied the effect of

the size of those nanomaterials on their antifungal activity. Three different concentrations (5, 10 and 20 ppm) of size controlled AgNPs ( $45.2 \pm 0.5$  nm,  $30 \pm 1.5$  nm and  $12 \pm 0.5$  nm) biosynthesized using the endophytic fungus *A. terrus* at different pH and temperature conditions were analyzed in PDA plates against three pathogenic of *Alternaria solani* isolates, the causal agent of tomato early blight disease. The results indicated the ability of all tested AgNPs to inhibit *A. solani* mycelial growth to various degrees (Table 2; Figure 10).

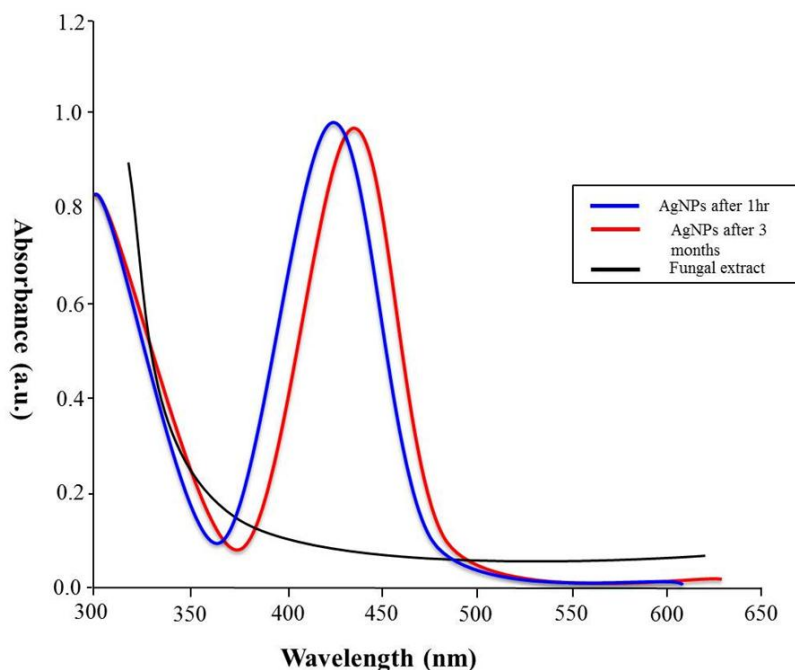


Figure 9: Evaluation of stability of the biosynthesized AgNPs after 1 month later of optimization.

The AgNPs with  $12 \pm 0.5$  nm (Figure 10C), followed by AgNPs with  $30 \pm 1.5$  nm size (Fig. 10B), showed better antifungal activity against *A. solani*, compared with AgNPs with  $45.2 \pm 0.5$  nm (Figure 10A). These results means that as the AgNPs become smaller in

size, their antifungal activity become more potent, as previously reported (Ajitha et al., 2015; Khaydarov & Khaydarov, 2009). This finding indicates the strong antifungal activity of the AgNPs biosynthesized under controlled conditions and its potential use as an

alternative to synthetic fungicides (Mohamed, 2015; Dubey et al., 2009; Stoimenov et al., 2002). Several studies reported the multiple modes of inhibitory action of AgNPs against diverse

microbial pathogens, however the exact antimicrobial mechanism of these nanoparticles is still not fully understood (Kim et al., 2009; Sondi & Salopek-Sondi, 2004).

Table 2: Mean of inhibitory growth rate (%) of three pathogenic *Alternaria solani* isolates treated by the different controlled sized and concentrations of AgNPs.

| Pathogen                        | AgNPs size    | Inhibition rate (%) |           |           |
|---------------------------------|---------------|---------------------|-----------|-----------|
|                                 |               | 5ppm                | 10ppm     | 20ppm     |
| <i>A. solani</i> F11 (KT721909) | 45.2 ± 0.5 nm | 66.7±0.02           | 70.0±0.01 | 72.9±0.01 |
|                                 | 30.0 ± 1.5 nm | 71.5±0.02           | 84.0±0.01 | 92.5±0.01 |
|                                 | 12.0 ± 0.5 nm | 81.4±0.01           | 90.1±0.01 | 96.9±0.02 |
| <i>A. solani</i> F12 (KT721910) | 45.2 ± 0.5 nm | 65.0±0.04           | 72.2±0.02 | 77.8±0.04 |
|                                 | 30.0 ± 0.5 nm | 71.4±0.01           | 82.4±0.02 | 90.3±0.04 |
|                                 | 12.0 ± 0.5 nm | 79.6±0.02           | 88.3±0.01 | 96.0±0.01 |
| <i>A. solani</i> F14 (KT721911) | 45.2 ± 0.5 nm | 68.6±0.02           | 74.4±0.02 | 80.5±0.04 |
|                                 | 30.0 ± 0.5 nm | 75.6±0.04           | 80.6±0.01 | 87.1±0.02 |
|                                 | 12.0 ± 0.5 nm | 81.5±0.02           | 89.5±0.01 | 95.6±0.02 |

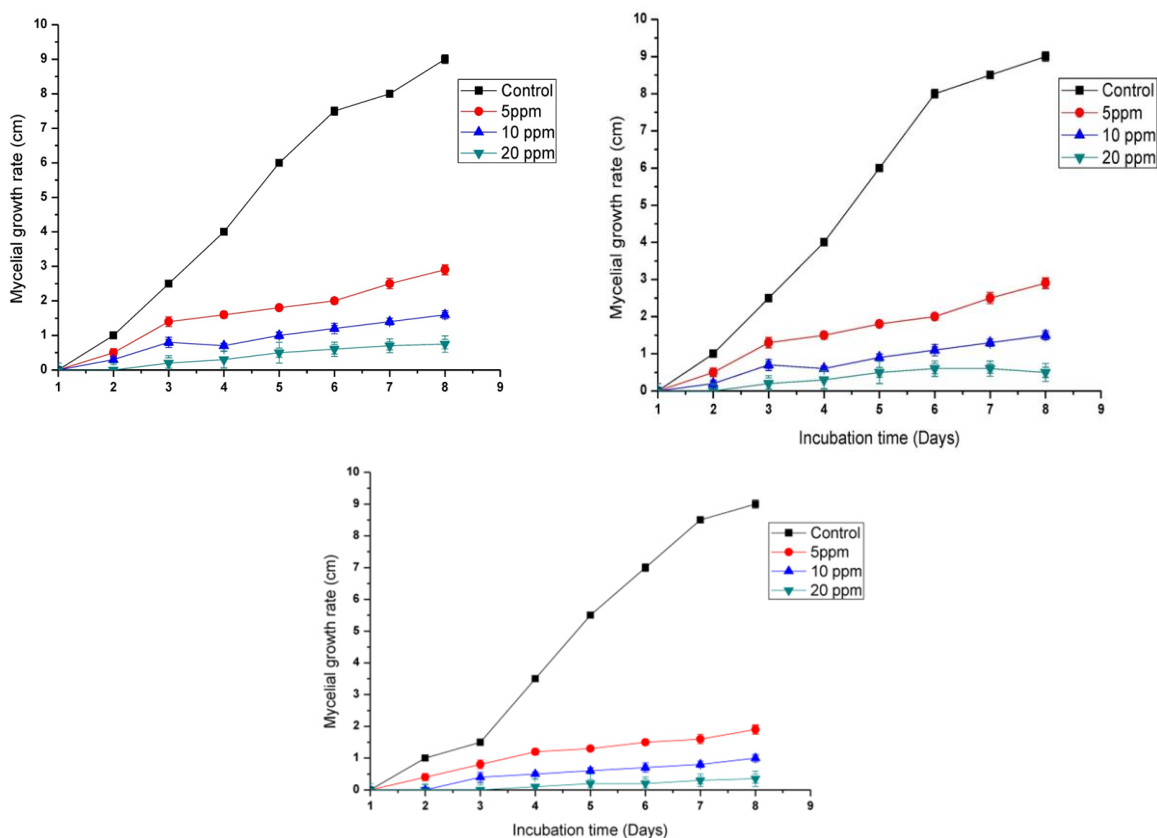


Figure 10: Antifungal effect of different controlled size biologically synthesized AgNPs at different concentrations (5, 10 and 20 ppm) on the mycelial growth rate of the pathogenic *A. solani* F11 (KT721909); AgNPs with (A) 45.2± 0.5 nm (B) 30± 1.5 nm and (C) 12± 0.5 nm size.

However, Kim et al. (2009) suggested that this may be backed to the unique ability of AgNPs to form free radicals that could disturb microbe membrane lipids and spoil their membrane functions (Mohamed, 2015). Other works suggested that the microbial membrane can be destroyed by the formation of pits on the surface of the cell wall membrane and disrupt the fungal transport systems through ion efflux (Pingali et al., 2005; Stoimenov et al., 2002). This leads to increased cell permeability and disturbed the ion transport in the cell system, which results in final cell death (Pingali et al., 2005). Hence biogenesis of AgNPs under controlled conditions is a good unique straightforward route that is easily produced and can prove extensively useful in plant disease management. Silver nanoparticles of different sizes and high stability were synthesized using simple, low cost and eco-friendly green chemistry approach. In the present study, the aqueous extract of the endophytic fungus *Aspergillus terreus* F37 (KX024595) was used as reducing/capping agent in the AgNPs synthesis. This single step procedure is highly suitable for large scale production as it is more cheap, economic, rapid and eliminates the elaborate processes employed in the other bio-based protocols. The characterization of AgNPs by UV-vis spectroscopy, TEM, XRD, DLS and FTIR biosynthesized under laboratory conditions showed that the formed AgNPs were spherical in shape, crystalline in nature. Average size of the silver nanoparticles was tunable by simply changing pH of the reactions. The optimum conditions for maximum production of small control sized AgNPs were pH (10) and temperature (100 °C)

which confirmed by DLS analysis. The AgNPs became more spherical-like in shape after being heated at 100 °C for two hours due to the promoted intra-particle ripening. After the aging treatment, spherical AgNPs with sizes of  $12 \pm 0.5$  nm could be successfully acquired from the products prepared under different pH. Interestingly, all the controlled small sized AgNPs exhibited excellent antifungal activity against *A. solani* the causal agent of tomato early blight disease at comparatively low concentration (5, 10 and 20) ppm and reduced their viability in a pH dependent manner. Based on those findings, it is concluded that AgNPs could be used as an antifungal agent in controlling various plant diseases caused by fungi. However, it further study are in need to clearly understand the exact mechanism by which silver nanoparticles control the fungal pathogen.

### Acknowledgements

Financial support from the European Commission through the Erasmus Mundus Scholarship-ACTION 2 WELCOME programme is gratefully acknowledged. Work in the JAD laboratory was supported by Grant BIO2014-54269-R from the Spanish Ministerio Economía y Competividad (MINECO, Spain).

### References

- Abd-Alla MH, Nafady NA, Khalaf DM, 2016. Assessment of silver nanoparticles contamination on faba bean-*Rhizobium leguminosarum* bv. *viciae*-*Glomus aggregatum* symbiosis: Implications for

- induction of autophagy process in root nodule. *Agriculture, Ecosystems & Environment* **218**: 163–177.
- Abdel-Hafez SI, Nafady NA, Abdel-Rahim IR, Shaltout AM, Mohamed MA, 2016a. Biogenesis and Optimisation of Silver Nanoparticles by the Endophytic Fungus *Cladosporium sphaerospermum*. *International Journal of Nanomaterials and Chemistry* **2**(1): 11–19.
- Abdel-Hafez SI, Nafady NA, Abdel-Rahim IR, Shaltout AM, Daròs J A, Mohamed MA, 2016b. Assessment of protein silver nanoparticles toxicity against pathogenic *Alternaria solani*. *3 Biotech* **6**(2): 199.
- Ahmadi TS, Wang ZL, Green TC, Henglein A, El-Sayed MA, 1996. Shape-controlled synthesis of colloidal platinum nanoparticles. *Science* **272**(5270): 1924.
- Ajitha B, Reddy YAK, Reddy PS, 2015. Enhanced antimicrobial activity of silver nanoparticles with controlled particle size by pH variation. *Powder Technology* **269**: 110–117.
- Azizi S, Namvar F, Mahdavi M, Ahmad MB, Mohamad R, 2013. Biosynthesis of silver nanoparticles using brown marine macroalga, *Sargassum muticum* aqueous extract. *Materials* **6**: 5942–5950.
- Baghizadeh A, Ranjbar S, Gupta VK, Asif M, Pourseyedi S, Karimi MJ, Mohammadinejad R 2015. Green synthesis of silver nanoparticles using seed extract of *Calendula officinalis* in liquid phase. *Journal of Molecular Liquids* **207**: 159–163.
- Borneman J, Hartin JR, 2000. PCR primers that amplify fungal rRNA genes from Environmental samples. *Applied and Environmental microbiology* **66**: 4356–4360.
- Cordero T, Mohamed MA, López-Moya JJ, Daròs, JA, 2017. A Recombinant Potato virus Y Infectious Clone Tagged with the Roseal Visual Marker (PVY-Ros1) Facilitates the Analysis of Viral Infectivity and Allows the Production of Large Amounts of Anthocyanins in Plants. *Frontiers in microbiology* **8**: 611.
- Dewi RT, Tachibana S, Dewi P, Kardono LBS, Ilyas M, 2014. Isolation of Bioactive Compounds from *Aspergillus terreus* LS07. *Indonesian Journal of Chemistry* **14**(3): 304–310.
- Dubey M, Bhadauria S, Kushwah B, 2009. Green synthesis of nanosilver particles from extract of *Eucalyptus hybrida* (safeda) leaf. *Digest Journal of Nanomaterials and Biostructures* **4**: 537–543.
- Escárcega-González CE, Garza-Cervantes JA, Vázquez-Rodríguez A, Montelongo-Peralta L Z, Treviño-González MT, Castro EDB, Rosales JC, 2018. *In vivo* antimicrobial activity of silver nanoparticles produced via a green chemistry synthesis using *Acacia rigidula* as a reducing and capping agent. *International journal of nanomedicine* **13**: 2349.
- Evanoff, DD, Chumanov G, 2004. Size-controlled synthesis of nanoparticles. 1. “Silver-only” aqueous suspensions via hydrogen reduction. *The Journal of Physical Chemistry B* **108**(37): 13948–13956.
- Gardes M, Bruns TD, 1993. ITS primers with enhanced specificity for basidiomycetes-application to the identification of mycorrhizae and rusts, *Molecular Ecology*, **2**(2): 113–118.

- Iravani S, 2011. Green synthesis of metal nanoparticles using plants. *Green Chemistry* **13**(10): 2638–2650.
- Ji X, Song X, Li J, Bai Y, Yang W, Peng X, 2007. Size control of gold nanocrystals in citrate reduction: the third role of citrate. *Journal of the American Chemical Society* **129**(45): 13939–13948.
- Khatami M, Sharifi I, Nobre MA, Zafarnia N, Aflatoonian MR, 2018. Waste-grass-mediated green synthesis of silver nanoparticles and evaluation of their anticancer, antifungal and antibacterial activity. *Green Chemistry Letters and Reviews* **11**(2): 125–134.
- Kathiravan V, Ravi S, Ashokkumar S, Velmurugan S, Elumalai K, Khatiwada CP, 2015. Green synthesis of silver nanoparticles using *Croton sparsiflorus* morong leaf extract and their antibacterial and antifungal activities. *Spectrochimica Acta Part A: Molecular and Biomolecular Spectroscopy* **139**: 200–205.
- Khaydarov RA, Khaydarov RR, Gapurova O, Estrin Y, Scheper T, 2009. Electrochemical method for the synthesis of silver nanoparticles. *Journal of Nanoparticle Research* **11**(5): 1193–1200.
- Kim KJ, Sung WS, Suh BK, Moon SK, Choi JS, Kim JG, Lee DG, 2009. Antifungal activity and mode of action of silver nano-particles on *Candida albicans*. *Biometals* **22**(2): 235–242.
- Kim SW, Jung JH, Lamsal K, Kim YS, Min JS, Lee YS, 2012. Antifungal effects of silver nanoparticles (AgNPs) against various plant pathogenic fungi. *Mycobiology* **40**(1): 53–58.
- Kumar CG, Sujitha P, 2014. Green synthesis of Kocuran-functionalized silver glyconanoparticles for use as antibiofilm coatings on silicone urethral catheters. *Nanotechnology* **25**(32): 325101.
- Liu L, Yang J, Xie J, Luo Z, Jiang J, Yang YY, Liu S, 2013. The potent antimicrobial properties of cell penetrating peptide-conjugated silver nanoparticles with excellent selectivity for Gram-positive bacteria over erythrocytes. *Nanoscale* **5**(9): 3834–3840.
- Lu L, Kobayashi A, Tawa K, Ozaki Y, 2006. Silver nanoplates with special shapes: controlled synthesis and their surface plasmon resonance and surface-enhanced Raman scattering properties. *Chemistry of materials* **18**(20): 4894–4901.
- Mallick K, Witcomb M, Scurrill M, 2006. Silver nanoparticle catalysed redox reaction: an electron relay effect. *Materials Chemistry and Physics* **97**(2): 283–287.
- McFarland AD, Van Duyne RP, 2003. Single silver nanoparticles as real-time optical sensors with zeptomole sensitivity. *Nano letters* **3**(8): 1057–1062.
- Mittal, AK, Chisti Y, Banerjee UC, 2013. Synthesis of metallic nanoparticles using plant extracts. *Biotechnology Advances* **31**: 346–356.
- Mohamed MA, 2015. One-Step Functionalization of Silver Nanoparticles Using the Orsellinic Acid Compound Isolated From the Endophytic Fungus *Epicoccum Nigrum*: Characterization and Antifungal Activity. *International Journal of Nanomaterials and Chemistry* **1**: 103–110.

- Mohamed AEMA, Mohamed MA, Vega V, Hernando B, Ahmed AM, 2016. Tuning magnetoresistive and magnetocaloric properties via grain boundaries engineering in granular manganites. *Rsc Advances* **6**(81): 77284–77290.
- Morones JR, Elechiguerra JL, Camacho A, Holt K, Kouri JB, Ramírez JT, Yacaman MJ, 2005. The bactericidal effect of silver nanoparticles. *Nanotechnology* **16**: 2346–23453.
- Morsy FM, Nafady NA, Abd-Alla MH, Elhady DA, 2014. Green synthesis of silver nanoparticles by water soluble fraction of the extracellular polysaccharides/matrix of the cyanobacterium *Nostoc commune* and its application as a potent fungal surface sterilizing agent of seed crops. *Universal Journal of Microbiology Research* **2**: 36–43.
- Ni PA, Hassan EW Kaler, 2005. Structural characteristics and growth of pentagonal silver nanorods prepared by a surfactant method. *Langmuir* **21**: 3334–3337.
- Noguez C, 2007. Surface plasmons on metal nanoparticles: the influence of shape and physical environment. *The Journal of Physical Chemistry C* **111**(10): 3806–3819.
- Panáček A, Kvitek L, Pucek R, Kolar M, Vecerova R, Pizurova N, Zboril R, 2006. Silver colloid nanoparticles: synthesis, characterization, and their antibacterial activity. *The Journal of Physical Chemistry B* **110**(33): 16248–16253.
- Petrini O, Fisher PJ, 1988. A comparative study of fungal endophytes in xylem and whole stems of *Pinus sylvestris* and *Fagus sylvatica*. *Transactions of the British Mycological Society* **91**(2): 233–238.
- Phithiviraj B, Singh UP, Singhk P et al, 1998. Field evaluation of ajoene, a constituent of garlic (*Allium sativum*) and neemazal, a product of neem (*Azadirachta indica*) for the control of powdery mildew (*Erysiphe pisi*) of pea (*Pisum sativum*). *Journal of Plant Diseases and Protection* **105**(3): 274–278.
- Pillai ZS, Kamat PV, 2004. What factors control the size and shape of silver nanoparticles in the citrate ion reduction method?. *The Journal of Physical Chemistry B* **108**(3): 945–951.
- Pingali KC, Rockstraw DA, Deng S, 2005. Silver nanoparticles from 445 ultrasonic spray-pyrolysis of aqueous silver nitrate. *Aerosol science and technology* **39**: 1010–1014.
- Qian Y, Yu H, He D, Yang H, Wang W, Wan X, Wang L, 2013. Biosynthesis of silver nanoparticles by the endophytic fungus *Epicoccum nigrum* and their activity against pathogenic fungi. *Bioprocess Biosystem Engineering* **36**: 1613–1619.
- Qin Y, Ji X, Jing J, Liu H, Wu H, Yang W, 2010. Size control over spherical silver nanoparticles by ascorbic acid reduction. *Colloids and Surfaces A: Physicochemical and Engineering Aspects* **372**(1): 172–176.
- Reddy NJ, Vali DN, Rani M, Rani SS, 2014. Evaluation of antioxidant, antibacterial and cytotoxic effects of green synthesized silver nanoparticles by *Piper longum* fruit. *Materials Science and Engineering C* **34**: 115–122.
- Roopan SM, Madhumitha G, Rahuman AA, Kamaraj C, Bharathi A, Surendra TV, 2013. Low-cost and eco-friendly phyto-synthesis of silver nanoparticles using *Cocos nucifera* coir extract and its

- larvicidal activity. *Industrial Crops and Products* **43**: 631–635.
- Sherry LJ, Chang SH, Schatz GC, Van Duynne, RP, Wiley BJ, Xia Y, 2005. Localized surface plasmon resonance spectroscopy of single silver nanocubes. *Nano letters* **5**(10): 2034–2038.
- Shrivastava S, Bera T, Roy A, Singh G, Ramachandrarao P, Dash D, 2007. Characterization of enhanced antibacterial effects of novel silver nanoparticles. *Nanotechnology* **18**(22): 225103.
- Siddique YH, Fatima A, Jyoti S, Naz F, Khan W, Singh BR, Naqvi AH, 2013. Evaluation of the toxic potential of graphene copper nanocomposite (GCNC) in the third instar larvae of transgenic *Drosophila melanogaster* (hsp70-lacZ) Bg 9. *PLoS ONE* **8**(12): e80944.
- Slistan-Grijalva A, Herrera-Urbina R, Rivas-Silva JF, Avalos-Borja M, Castellón-Barraza F F, Posada-Amarillas A, 2005. Classical theoretical characterization of the surface plasmon absorption band for silver spherical nanoparticles suspended in water and ethylene glycol. *Physica E: Low-dimensional Systems and Nanostructures* **27**(1): 104–112.
- Sondi I, Salopek-Sondi B, 2004. Silver nanoparticles as antimicrobial agent: a case study on *E. coli* as a model for Gram-negative bacteria. *Journal of Colloid Interface Science* **275**: 177–182.
- Sondi I, Goia DV, Matijević E, 2003. Preparation of highly concentrated stable dispersions of uniform silver nanoparticles. *Journal of Colloid and Interface Science* **260**(1): 75–81.
- Song W, Ma X, Tan H, Zhou J, 2011. Abscisic acid enhances resistance to *Alternaria solani* in tomato seedlings. *Plant Physiology and Biochemistry* **49**(7): 693–700.
- Stoimenov PK, Klinger RL, Marchin GL, Klabunde KJ, 2002. Metal Oxide Nanoparticles as Bactericidal Agents. *Langmuir* **18**: 6679–6686.
- Tanvir S, Oudet F, Pulvin S, Anderson WA, 2012. Coenzyme based synthesis of silver nanocrystals. *Enzyme and Microbial Technology* **51**(4): 231–236.
- Velikov KP, Zegers GE, Van Blaaderen A, 2003. Synthesis and characterization of large colloidal silver particles. *Langmuir* **19**(4): 1384–1389.
- Wiley BJ, Im SH, Li ZY, McLellan J, Siekkinen A, Xia Y, 2006. Maneuvering the surface plasmon resonance of silver nanostructures through shape-controlled synthesis. *The Journal of Physical Chemistry B* **110**(32): 15666–15675.
- Dong X, Ji H, Wu L, Zhao J, Li Yang W, 2009. Shape control of silver nanoparticles by stepwise citrate reduction, *Journal of Physical Chemistry C* **113**: 6573–6576.
- Zachariadis PC, Hadjikakou SK, Hadjiliadis N, Skoulika S, Michaelides A, Balzarini J, De Clercq E, 2004. Synthesis, characterization and *in vitro* study of the cytostatic and antiviral activity of new polymeric silver (I) complexes with ribbon structures derived from the conjugated heterocyclic thioamide 2-mercapto-3, 4, 5, 6-tetra-hydropyrimidine. *European Journal of Inorganic Chemistry* **7**:1420–1426.

Zhang Y, Tan YW, Stormer HL, Kim P, 2005. Experimental observation of the quantum Hall effect and Berry's phase in graphene. *Nature* **438**(7065): 201–204.